

Modelling the surface generation process during AFM probe-based machining: simulation and experimental validation

This content has been downloaded from IOPscience. Please scroll down to see the full text.

2014 Surf. Topogr.: Metrol. Prop. 2 025001

(<http://iopscience.iop.org/2051-672X/2/2/025001>)

View [the table of contents for this issue](#), or go to the [journal homepage](#) for more

Download details:

IP Address: 131.251.254.28

This content was downloaded on 07/03/2014 at 11:59

Please note that [terms and conditions apply](#).

Modelling the surface generation process during AFM probe-based machining: simulation and experimental validation

A Elkaseer^{1,2} and E B Brousseau¹

¹ Cardiff School of Engineering, Cardiff University, Cardiff, UK

² Production Engineering and Mechanical Design Department, Faculty of Engineering, Port Said University, Port Said, Egypt

E-mail: BrousseauE@cf.ac.uk

Received 5 July 2013, revised 31 October 2013

Accepted for publication 20 November 2013

Published 23 December 2013

Abstract

The controlled removal of material conducted with the tip of an atomic force microscope (AFM) probe is a technique that has started gaining increased attention in recent years within the micro and nano manufacturing research community. The attractive characteristics of this process are that it is relatively simple to implement and low-cost compared with vacuum-based lithography techniques for micro and nano fabrication. However, similarly to any machining process, the resulting surface finish of features cut with an AFM probe can be critical. In this context, the focus of the paper is on the development and validation of a novel analytical model for predicting the floor surface roughness induced by AFM probe-based machining when generating cavities composed of linear parallel grooves. In addition to kinematic parameters, the proposed model takes into account the minimum chip thickness and elastic recovery associated with each phase present within the microstructure of a workpiece. The implementation of the model was carried out and its performance tested when processing a dual phase brass alloy using an AFM nano-indentation probe. A relatively good agreement was achieved between the analytical and experimental results with an average prediction error of 21% when assessing the arithmetic average roughness, Ra.

Keywords: atomic force microscopy, probe-based machining, surface roughness

1. Introduction

Mechanical machining with the tip of an atomic force microscope (AFM) probe is a particular implementation of the AFM scratching technique where material removal from the surface of a sample/workpiece occurs at nano-scale as a result of the direct contact between the tip of an AFM probe and the sample surface (see figure 1). However, while AFM scratching studies are generally confined to the generation of single grooves with the aim of assessing particular material properties near the surface, such as the scratch hardness (Beegan *et al* 2007) or the scratch resistance of thin films (Sundararajana and Bhushan 2001), AFM probe-based machining is specifically targeted at the controlled production of more complex structures. For instance, these features can

be single curvilinear grooves (Bourne *et al* 2010), pockets machined as a result of the probe tip cutting parallel and adjacent lines (Fang and Chang 2003) or arrays of nano-scale hemispherical pillars (Tseng *et al* 2011).

The AFM probe-based machining process is relatively simple and low-cost to implement (Gozen and Ozdoganlar 2012). In addition, it has shown high flexibility in producing complex three dimensional features and has been applied for cutting a wide range of engineering materials (Brousseau *et al* 2010). When this technique is employed to machine soft samples, such as polymers, the cutting operations can be performed with silicon or silicon nitride probes that would otherwise normally be used for imaging purposes (Blach *et al* 2004). For harder substrates, AFM probes designed for nano-indentation tasks and which are made of a pyramidal



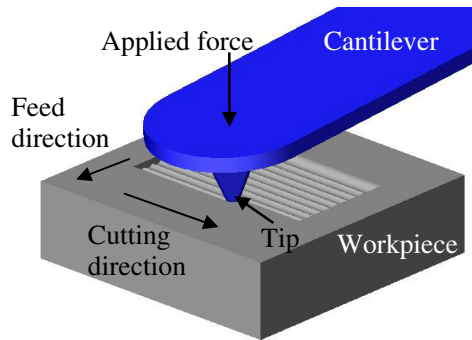


Figure 1. Schematic representation of the AFM probe-based mechanical machining process when producing a pocket.

diamond tip mounted on a stainless steel cantilever can be utilized (Yan *et al* 2009) as well as AFM tips that have been coated with diamond (Fang and Chang 2003) or carbon (Iwata *et al* 2003) to increase their life span. Although the range of probes that can possibly be used for AFM machining is relatively large, the radius of the tip which acts as the cutting edge typically exhibits values of between 10 and 100 nm. Thus, combined with the fact that AFM instruments possess nano-scale displacement resolution, AFM probe-based mechanical machining has been developed as a suitable technique for the generation of sub-micrometre features.

However, similarly to other machining processes, and especially those for micro- and nano-scale cutting, the resulting surface roughness of processed workpieces can be critical because it is not possible to easily apply follow-up processing techniques to improve its quality (Dornfeld *et al* 2006, Elkaseer *et al* 2012). Thus, it is important to develop suitable models of the AFM probe-based machining process for predicting the achievable surface roughness and, as a result, for identifying optimized processing windows. In the case of micro milling, where the tools utilized typically have a cutting edge radius a hundred times larger than that of an AFM probe (i.e. between 1 and 10 μm), it is known that, due to scale effects, it is not sufficient to consider kinematic parameters only when modelling the surface generation process (Vogler *et al* 2004, Liu and Melkote 2006). Similarly, when studying AFM probe-based mechanical machining, other factors which dominate the underlying cutting mechanism, such as the mechanical properties of the workpiece material, have to be considered to predict the roughness of machined surfaces.

In this context, the aim of this research is to develop a model of the surface generation process during AFM probe-based machining by obtaining a deeper understanding of the physical phenomena that influence the resulting topography of the surfaces that have been machined. To achieve this, it is proposed that the mechanical properties of each phase present within a material microstructure are examined in order to take them into account in the model. This is particularly required in order to assess and quantify the influence of some of the machining characteristics associated

with a given workpiece material, especially the minimum chip thickness and the elastic recovery of each phase. The paper is organized as follows. The next section provides a review of existing modelling approaches that have been developed to predict the surface topography generated with single point precision cutting methods. Next, a novel surface generation model is presented and the experimental trials used to implement it are described. Then, a comparison between the model predictions and experimental results are reported and discussed. Finally, conclusions and perspective are given in the last section.

2. The modelling of surface generation for single point precision machining

Material removal at nano-scale generated under the mechanical action of a cutter on a workpiece has been a topic of research for many years and started even prior to the invention of the AFM through the efforts of the machining research community in developing methods for precision cutting. For instance, single point diamond turning (SPDT) machines were initially developed in the early 1980s (Wills-Moreen *et al* 1982, Donaldson and Patterson 1983) while the AFM technology was first introduced a few years later for the primary purpose of imaging and characterizing specimens at the nano-scale (Binnig *et al* 1986). The type of produced structures is one of the important differentiating factors between AFM probe-based machining and precision turning techniques. More specifically, the AFM probe-based material removal process is focussed on the generation of discrete features with high spatial resolution while precision machining is aiming at the production of relatively large surfaces characterized with nanometre scale form accuracy and surface finish. In spite of this, with respect to modelling the surface topography created by a cutting tool across a machined surface, both techniques share similarities. In particular, and as illustrated in figure 1 in the case of AFM probe-based machining, the generated roughness in the feed direction can be modelled as the cross section of a series of parallel grooves that are cut by a V-shaped tool having an edge radius where contact with the workpiece occurs. Thus, for modelling the surface generation of micro/nano cavities produced with AFM cutting, or that of large areas processed with precision machining, the common objective is to accurately predict the shape of the created grooves and the intersection point or profile between two consecutive grooves.

For the process of finish turning, where small values of uncut chip thickness and feed are utilized, it is well known that estimating the generated surface roughness based only on kinematic parameters (i.e. the tool nose geometry and tool feed) leads to an underestimation of the measured roughness. Brammertz (1961) proposed a formula to estimate the theoretical ten-point height roughness that takes into account the minimum undeformed chip thickness in addition to the kinematic parameters. In this way, the intersection between two consecutive machined grooves was characterized by a small triangular area that could not be cut due to its thickness being smaller than a minimum thickness.

Grzesik (1996) subsequently revised Brammertz's model by considering variations of the minimum undeformed chip thickness as a function of the tool feed. More recently, Liu and Melkote (2006) presented a model for predicting the surface roughness in micro-turning of an Al5083-H116 alloy by taking into account the effects of plastic side flow, tool geometry and process parameters. In particular, these authors showed that the commonly observed discrepancy between the theoretical and measured surface roughness in micro-turning is mainly due to surface roughening caused by plastic side flow.

Cheung and Lee (2000) developed a model of the ultra-precision turning process to predict the surface topography in the feed direction of machined parts. The model was built by taking into account the tool geometry, the feed rate and the relative vibration between the tool and the workpiece while assuming that the processed material was homogeneous and isotropic. In a subsequent study, the same authors used the power spectrum analysis method to correlate surface roughness profiles to the different process parameters considered in their model (Cheung and Lee 2001). This analysis led to the identification of additional factors that have an influence on the surface generation process in SPDT. In particular, tool interference and a mechanism reported by these authors as material swelling were found to be important process characteristics that affect the resulting surface finish. Tool interference is caused by process vibrations and is characterized by material along the current path of the cutting tool that has already been removed by the preceding cut. The so-called material swelling is a result of plastic flow of material being pushed out on the edge of a groove and can also be referred to as pile-up. It was also observed by these authors that the presence of such pile-ups contributed to explain the under-estimation of the surface roughness predicted by their model compared to the experimental results obtained when machining an aluminium alloy. Luo *et al* (2005) developed a more complex model of the surface generation process in precision turning by taking into account regenerative chatter, cutting tool characteristics, time-dependent cutting forces and the machine tool response. Similarly to the work reported by Cheung and Lee, the machined surface topography in the feed direction was derived by calculating intersection points between succeeding tool paths that had been computed *a priori* based on the different model parameters considered. This model was further refined by Zhou and Cheng (2009), where a number of additional nonlinear factors associated with the workpiece material, cutting process and machine tool performance were taken into account. The effects of nonlinear factors on the surface generation were analysed through the power spectral density method and were found to contribute more than 80% to the resulting surface roughness.

Other researchers have focused their efforts on modelling single point machining, not in the tool feed direction, as is the case for the studies reported above, but in the main cutting direction (i.e. along the tool path). To achieve this, molecular dynamics (MD) simulation has been a popularly used modelling approach (Zhang and Tanaka 1997, Komanduri *et al* 2000, Luo *et al* 2003, Ye *et al* 2003). MD simulation

performs analysis based on interatomic force calculations. In spite of the fact that the length of cut commonly investigated with MD analysis is restricted to a few nm due the high computational power required, this technique has enabled the study of nanometric cutting phenomena. In particular, using MD simulation, Zhang and Tanaka (1997) theoretically observed that, depending on the processing conditions, four distinct regimes can take place when sliding a moving diamond asperity with a tip radius of a few nm over a single crystal copper surface, namely: no-wear, adhering, ploughing and cutting. The transition between these regimes is governed by the tip radius, the speed and the engagement depth of the diamond asperity, as well as the degree of lubrication or contamination at the diamond–metal interface. In the no-wear and adhering regimes, only elastic deformation takes place while plastic deformation occurs in the other two regimes. The ploughing regime is characterized by the workpiece material being pushed out on the edges of a machined groove while the cutting regime results in chip formation.

Given the limitation of MD approaches with respect to the very short length of cut that can be investigated and the fact that in single point precision machining the surface roughness in the tool feed direction is more dominant than that in the main cutting direction (Cheung and Lee 2000), a modelling philosophy that aims at predicting intersection points or profiles between consecutive grooves is followed in this research. When machining with an AFM instrument, however, the range of cutting speeds generally achieved is below $100 \mu\text{m s}^{-1}$ and are, therefore, much lower than those conventionally applied in precision cutting. For this reason, dynamic effects are not taken into account in this study because they are not expected to contribute to the roughness generated during AFM probe-based machining. However, size effects, which are responsible for the discrepancy between the achieved roughness and the kinematic roughness, should be considered. In particular, for micro- and nano-scale cutting, the crystalline structure of processed materials has a significant influence on different machining characteristics, such as chip formation, surface generation and cutting forces (Weule *et al* 2001, Liu *et al* 2004). For example, it was shown by Vogler *et al* (2004) that the surface roughness values obtained when cutting multiphase ductile iron was larger than that for the single phase material over the examined range of cutting conditions. The increased surface roughness was attributed to interrupted chip formation that occurs as the cutting edge moves between the multiple phases. Unfortunately, no detailed study exists that takes into account the heterogeneity of a workpiece material for predicting the surface roughness generated in single point precision cutting, which could be directly applied for AFM probe-based machining. For this reason, the objective of this paper is to propose a predictive model to estimate the roughness achieved in the feed direction when cutting multiphase materials with the tip of an AFM probe by taking into account kinematic parameters as well as phase-specific parameters and, in particular, the minimum chip thickness and elastic recovery associated with each phase.

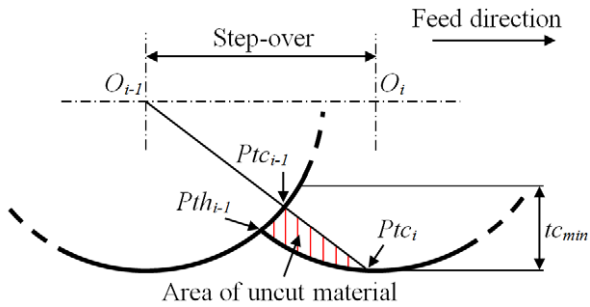


Figure 2. Surface generation in the feed direction during AFM probe-based machining.

3. Proposed surface roughness model

3.1. Model components

The developed model for surface roughness prediction in AFM probe-based machining consists of the following three components: the kinematic surface roughness, R_{th} ; the roughness contributed by the minimum chip thickness effect, R_{tc} and, that by the elastic recovery of the workpiece material, R_k .

The kinematic surface roughness, R_{th} , is defined as a periodic function, $z(x)$, as follows:

$$z(x) = \sqrt{r^2 - x^2} + r \quad \text{for } -\frac{f}{2} \leq x < \frac{f}{2} \quad \text{with } z(x+f) = z(x), \quad (1)$$

where z and x represent the vertical and horizontal coordinates of points comprised on the kinematic surface roughness profile, respectively; r is the tip edge radius and f is the distance between two consecutive grooves, which is also referred to as the step-over. Thus, based on these two kinematic parameters, the intersection point between two adjacent profiles is easily determined, as presented in figure 2. In particular, the theoretical intersection, $P_{th_{i-1}}$, between the cross sectional profile of the groove being cut, S_i , and the prior profile, S_{i-1} , is defined without considering material properties that influence the cutting mechanism.

Based on R_{th} , the roughness contributed by the minimum chip thickness effect, R_{tc} , is considered. As illustrated in figure 2, along the roughness profile in the feed direction, R_{tc} leads to an area of uncut material between two adjacent grooves. Thus, a new intersection point is calculated as follows in order to take into account the minimum chip thickness effect. First, a virtual line is created between the centre, O_{i-1} , of the arc defining the probe tip, and representing the prior cut profile, S_{i-1} , and a point P_{tc_i} located on the arc that determines the profile S_i of the groove currently being cut. In this way, the distance between the points $P_{tc_{i-1}}$ and P_{tc_i} , is also defined as shown on figure 2. In particular, for a given profile S_i being machined, $P_{tc_{i-1}}$ represents a point along the prior adjacent profile, S_{i-1} . Then, the distance $(P_{tc_{i-1}}, P_{tc_i})$ is compared with the minimum chip thickness value, t_{cmin} , for a given phase present within the material microstructure.

This leads to two possible cases:

- *Case 1.* $(P_{tc_{i-1}}, P_{tc_i}) < t_{cmin}$. In this case, ploughing is the prevailing machining mechanism and the segment $[P_{tc_{i-1}}, P_{tc_i}]$ belongs to the area of uncut chip thickness.
- *Case 2.* $(P_{tc_{i-1}}, P_{tc_i}) > t_{cmin}$. Here, cutting is the dominant condition and the point P_{tc_i} defines the end of the segment $[P_{tc_{i-1}}, P_{tc_i}]$ belonging to the surface at this position.

Thus, starting from point $P_{th_{i-1}}$, the profile S_{i-1} is explored until case 2 above is met. In addition, this analysis is conducted as a function of the particular phase being cut because the amplitude of the minimum chip thickness effect for fixed values of step-over and cutting edge is phase-dependent (Chuzhoy *et al* 2003a, 2003b, Vogler *et al* 2004). Thus, the area of uncut material depends on the minimum chip thickness value for a given phase processed and on the distance between two adjacent grooves.

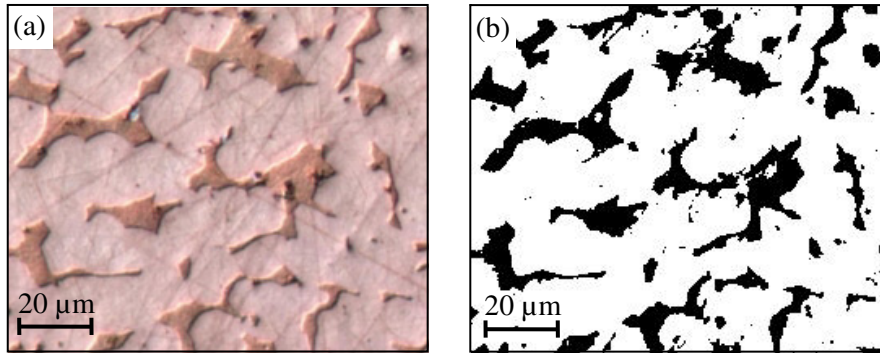
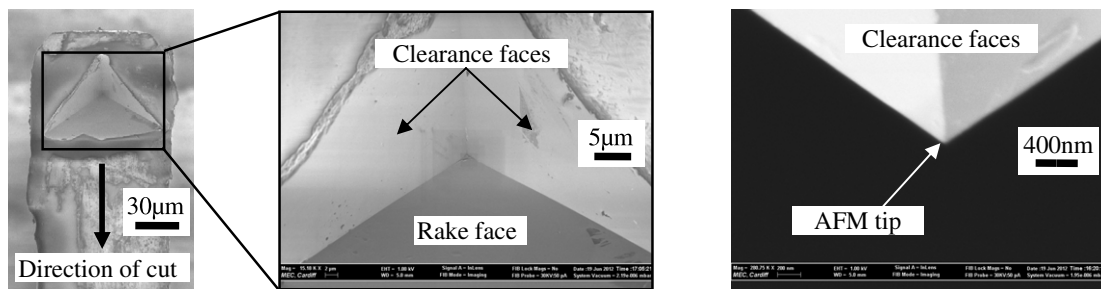
Finally, the property of elastic recovery for the different phases is considered due to the fact that uncut material, which has not been removed due to the minimum chip thickness effect, does not spring back fully to its original state (Liu *et al* 2007). For this reason, R_k , the roughness contribution from the elastic recovery characteristic of each phase, is introduced. In this case, the height of each point on the segment $[P_{tc_{i-1}}, P_{tc_i}]$ is multiplied by k , which is the elastic recovery for a given processed phase. The possible values for k are comprised between 0 and 1. Thus, the roughness calculated at this stage is always lower than R_{tc} assessed during the previous step.

3.2. Model implementation

The experimental investigations conducted in this research in order to implement the proposed model were carried out on a dual-phase material, CuZn₃₉Pb₃ brass alloy. A preliminary experiment was performed to examine the microstructure of this material through micro-hardness tests. In particular, micro-hardness measurements can give a first general indication about the mechanical properties of a material microstructure. In this case, an average was calculated from five different measurements conducted in each phase separately under a load of 10 g. For the α phase, the hardness was ~ 125 HV; however, for the β phase, it was ~ 203 HV. Thus, a difference in both the minimum chip thickness and the elastic recovery values between each phase is expected (Vogler *et al* 2003, Wang *et al* 2008). In addition, in order to account for the effect of the microstructure of a material when implementing the proposed model, the image processing technique presented by Elkaseer *et al* (2012) for mapping the microstructure of a workpiece surface was adapted to process AFM scan data. Such mapping data are then used as an input to feed the developed model for predicting the generated surface based on the type of phase at the in-progress position of the AFM tip. Figure 3 illustrates the material microstructure mapping procedure when using an optical micrograph of the surface of the CuZn₃₉Pb₃ brass alloy as the input data (see figure 3(a)).

Table 1. Parameters used for conducting the scratch tests in each phase.

	Minimum F_n (μN)	Maximum F_n (μN)	Length of cut (μm)	Cutting speed ($\mu\text{m s}^{-1}$)	Cutting direction
Groove 1	0	10	10	5	Towards the cantilever and parallel to its long axis
Groove 2	0	20			
Groove 3	0	30			
Groove 4	0	40			

**Figure 3.** Material microstructure mapping procedure, (a) optical micrograph of the $\text{CuZn}_{39}\text{Pb}_3$ brass alloy sample, (b) processed binary picture from the optical micrograph.**Figure 4.** Tip of the DNISP AFM probe.

To evaluate the kinematic surface roughness, R_{th} , the geometry of the AFM probe tip utilized must be characterized. A DNISP probe from Bruker was used in this study (see figure 4). This type of AFM probe is normally employed for nano-indentation experiments. It is made of a cantilever in stainless steel on which a three sided diamond tip is mounted. The particular AFM probe employed had a nominal normal spring constant of 209 N m^{-1} . In addition, the radius of the tip was measured using a scanning electron microscope (SEM) and found to be 70 nm.

Next, the minimum chip thickness value, as well as the elastic recovery of the phases to be cut, must be defined. A number of techniques for the evaluation of the minimum chip thickness have been proposed in the literature. The reported techniques are based on deterministic (Son *et al* 2005, Liu *et al* 2006), finite element (Vogler *et al* 2003) or experimental (Ikawa *et al* 1992) approaches. In this study, it was decided to take advantage of the available AFM instrumentation and, thus, to follow an experimental method

for determining these characteristics. In particular, the AFM offers the possibility of imaging and subsequently evaluating mechanical properties of each phase of the material within one set-up prior to performing cutting operations. More specifically, it is proposed to conduct *in situ* scratch tests of each phase present in the brass alloy to measure the minimum chip thickness and elastic recovery values according to the procedure described below.

Firstly, four grooves were machined in each phase. The force, F_n , applied by the DNISP probe tip onto the workpiece surface was increased linearly when cutting each groove. Table 1 provides a summary of the set-up used during these tests. Figure 5 shows an SEM image of the resulting grooves prior to cleaning the sample and, thus, the chips formed can also be observed in this figure. By using a set of CSG30 AFM probes from NT-MDT, which are designed for imaging purpose in contact mode, the height profile along the bottom of each groove could be obtained with the AFM instrument (see table 2).

Table 2. Profiles obtained along the length of each groove.

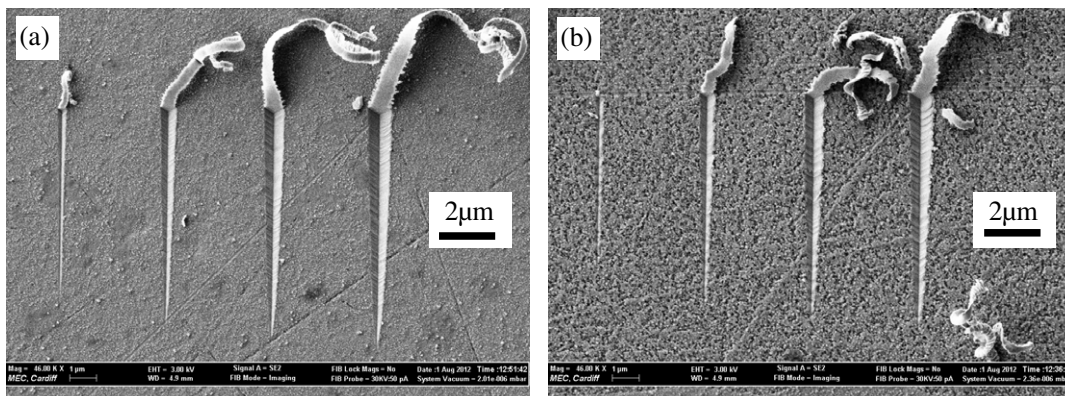
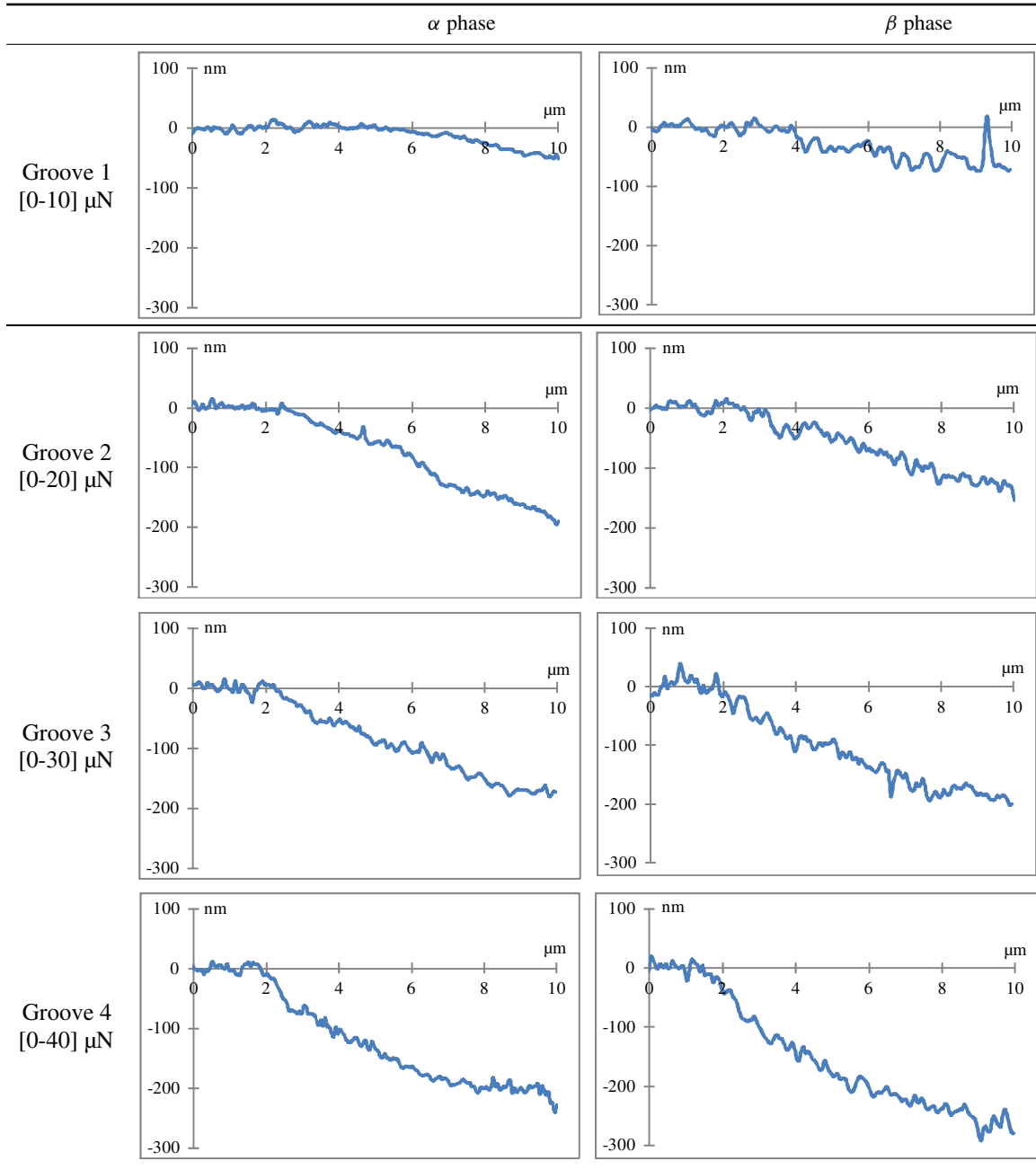


Figure 5. Scratch tests conducted to determine the minimum chip thickness and the elastic recovery of the (a) α phase and (b) β phase.

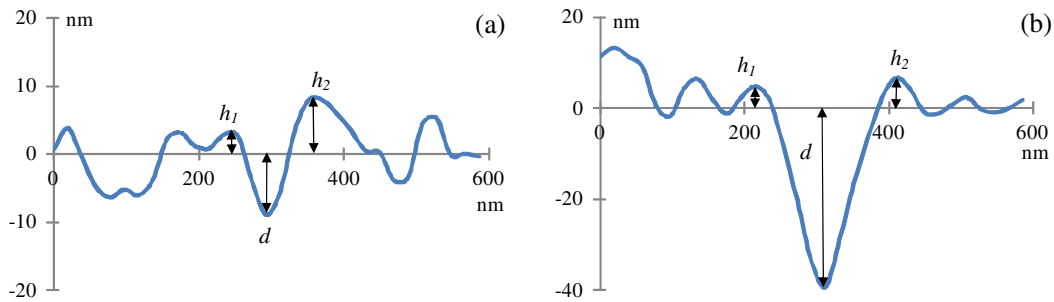


Figure 6. Examples of cross sections of a machined groove in the α phase at (a) the ploughing to cutting transition point and (b) under pure cutting mechanism.

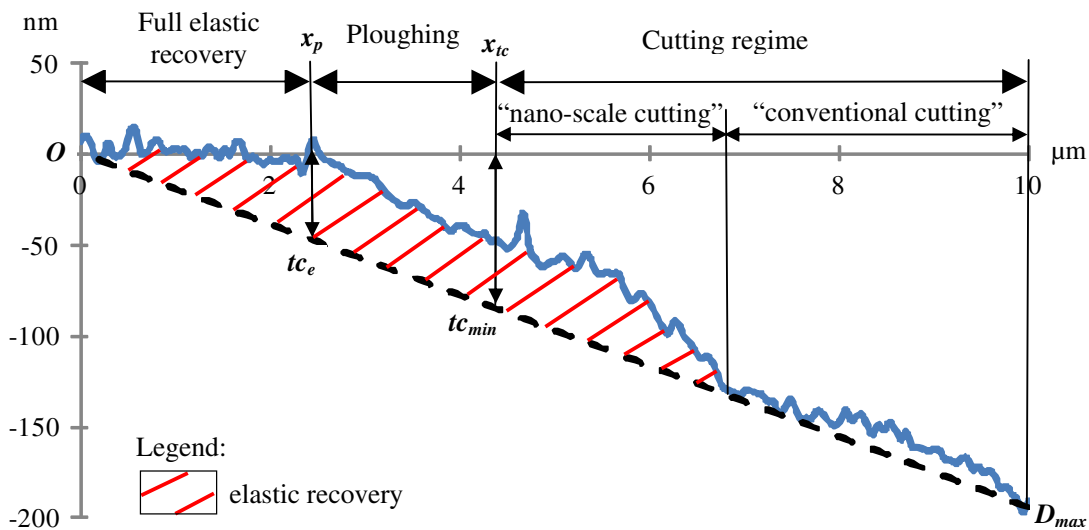


Figure 7. Illustration of the procedure used to determine the minimum chip thickness and the elastic recovery values for a particular scratched groove.

Secondly, the position along each groove at which the transition from ploughing to cutting occurs was determined and the chip-load at this point was considered to be equivalent to the minimum chip thickness for the assessed phase. As suggested by Ahn and Lee (2009), this transition was detected when the ratio between the sum of the pile-up heights measured on each side of a machined groove, h_1 and h_2 , and the depth of this groove, d , was less than one. Figure 6(a) shows an example of the cross section of a groove machined in the α phase that illustrates the transition between ploughing and cutting. In addition, the cross section along the same groove at a stage where the force applied, F_n , is higher and cutting is the regime dominating the machining mechanism, as given in figure 6(b). In practice, the adopted condition for detecting this transition from ploughing to cutting can be met on a number of neighbouring locations along a groove, which is due to the fact that there is some degree of uncertainty associated with this procedure as a result of the original roughness of the workpiece surface and the existence of a processing window where a mixing of both mechanisms is present. Thus, when analysing the different cross sections of a given groove in the direction of increased normal force, in

order to reduce the uncertainty in determining the start of the cutting regime, the transition point selected was that for which all subsequent points along the groove also met the condition.

Thirdly, for each groove, based on the profile data reported in table 2, a virtual line was created so that it joined the origin, O , where the depth of a groove equals zero and the point, D_{max} , corresponding to its maximum depth. This virtual line can be said to represent the theoretical depth of a groove should there be no occurrence of the minimum chip thickness and elastic recovery effects. From the beginning of a scratch test, where F_n is equal to zero until the end where F_n has increased linearly until reaching a maximum value, three regimes can be distinguished. In the first regime, F_n is too low to induce plastic deformation and, thus, a full elastic recovery of the material takes place. This corresponds to the no-wear and adhering regimes described in Zhang and Tanaka (1997). The second regime is characterized by ploughing as the main plastic deformation mechanism. Along the profile of a groove, the position which corresponds to the transition from pure elastic deformation (i.e. with full elastic recovery) to the ploughing regime can be determined

Table 3. Results for the experimental evaluation of the normalized minimum chip thickness, λ_n , and elastic recovery, k , for the α and β phases.

		Groove 1	Groove 2	Groove 3	Groove 4	Average	Standard deviation
α phase	λ_n	0.52	0.54	0.47	0.74	0.57	0.12
	k	0.71	0.36	0.37	0.83	0.57	0.24
β phase	λ_n	0.45	0.53	0.50	0.34	0.46	0.08
	k	0.77	1.00	0.79	0.95	0.88	0.12

Table 4. Parameters used for machining the pockets.

	Step-over (nm)	F_n (μN)	Cutting speed ($\mu\text{m s}^{-1}$)	Cutting direction
Pocket 1	80	12	5	Along the length of the pocket, towards and parallel to the long axis of the cantilever
Pocket 2	100			
Pocket 3	120			

by detecting where the groove starts being formed and it is referred to as x_p (see figure 7). The depth of the virtual line at this point is recorded as tc_e and it represents the minimum chip-load to induce plastic deformation. In the third regime, cutting is the dominant mechanism. In this case, F_n has reached a sufficient value for the engagement depth of the tip to be higher than the minimum chip thickness. Within this regime, as the ratio between the cutting depth and tip radius increases, the minimum chip thickness effect, and thus the amount of elastic recovery, decreases. At a certain point, the cutting phenomenon observed is similar to that of conventional cutting (Simoneau *et al* 2006, Mian *et al* 2010). This can be seen in figure 7, where the actual profile of the groove towards its end is close to the virtual line drawn. In general, a similar observation could also be made when analysing the other machined grooves. The position along a groove corresponding to the ploughing to cutting transition, x_{tc} , is determined based on the ratio of pile-up height to groove depth, as explained above. Based on this, the minimum chip thickness is calculated by measuring the theoretical depth, tc_{min} , along the virtual line at the position x_{tc} , as illustrated in figure 7. The difference between tc_{min} and the actual depth of the groove is due to the elastic recovery of the material. In particular, at the beginning of the cutting regime, a relatively substantial amount of elastic recovery is expected (Liu *et al* 2007). Thus, the normalized minimum chip thickness, λ_n , could be obtained for each groove by dividing tc_{min} by the radius of the tip, r .

Finally, the average elastic recovery, k , is calculated between the points x_p and x_{tc} (i.e. in the zone corresponding to the ploughing regime) according to the following equation:

$$k = \frac{1}{n} \sum_{i=1}^n \frac{d_{vi} - d_i}{d_{vi}}, \quad (2)$$

where d_{vi} is the depth along the virtual line and d_i is the actual depth of the groove profile at a given point i .

This procedure was applied on the AFM data obtained for each scratched groove and, thus, four measurements per phase could be conducted to identify λ_n and k . The individual measurements and their average obtained for both α and β phases are given in table 3.

From table 3, it is observed that a higher value of normalized minimum chip thickness was obtained when machining the α phase compared to the β phase under the same cutting conditions. This phenomenon is explained with differences in the mechanical properties between these two phases. In particular, the α phase is characterized by a higher toughness and lower hardness of ~ 125 HV, even when alloyed with a small quantity (up to about 10%) of zinc, which has no significant contribution to the hardening of the α phase. Therefore, ploughing can be the prevailing machining mechanism rather than cutting when compared with the response of the β phase under the same conditions, especially at low levels of applied tip penetration depth. At the same time, the β phase is more 'brittle' with a higher hardness of 203 HV, which in turn is associated with a lower minimum chip thickness (Wang *et al* 2008). Moreover, the results reflect the trade-off between the normalized minimum chip thickness and elastic recovery values obtained for the α and β phases, which again can be attributed to the difference in the mechanical properties of both phases. More specifically, the lower normalized minimum chip thickness value obtained for the β phase should contribute to a lower surface roughness compared to the α phase but, at the same time, its higher value of elastic recovery is opposing this effect. In general, it can be said that the results in table 3 provide evidence of the expected influence of the material microstructure on the underlying machining mechanism and, in turn, on the achieved surface quality.

The model described in this section was implemented in Matlab and its accuracy when machining pockets is analysed in the following section. In addition, the pseudo-code used to implement the proposed model and, thus, to determine the coordinates of points along the roughness profile in the feed direction is given in the [appendix](#).

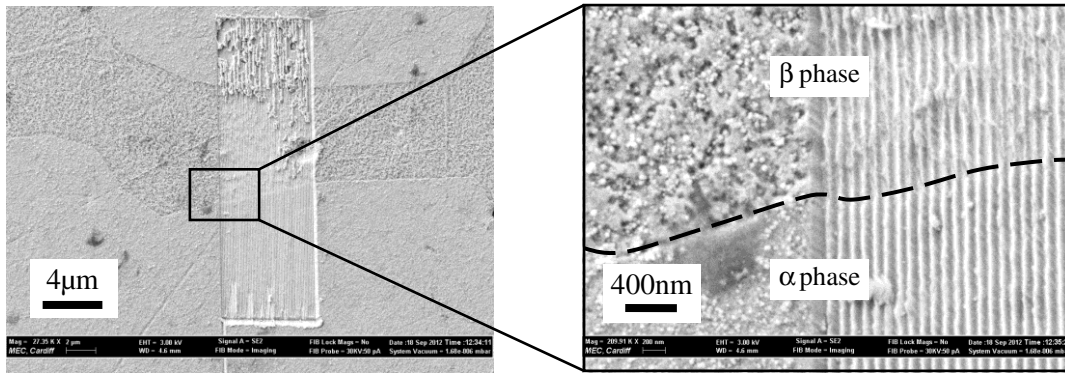


Figure 8. Example of a machined pocket with a step-over of 100 nm. The dashed line represents the boundary between the α and β phases.

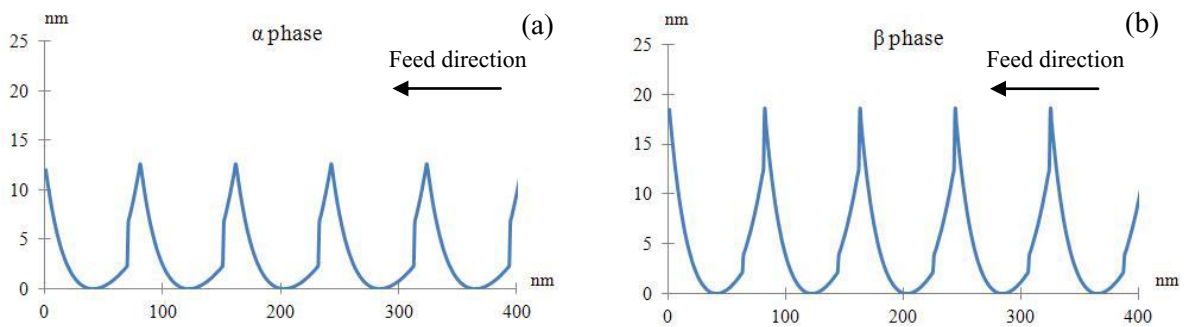


Figure 9. Predicted surface profile along the cross section of a series of parallel grooves with a step-over value of 80 nm for (a) the α phase and (b) the β phase.

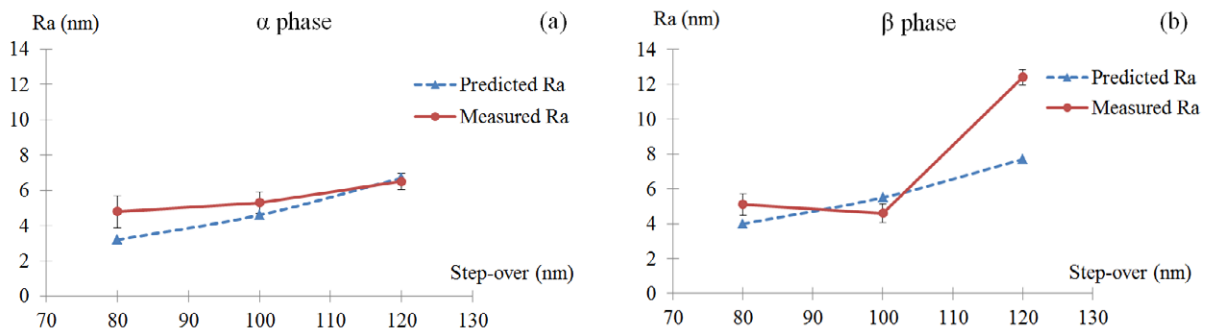


Figure 10. Experimental and predicted results for the arithmetic roughness, R_a , for (a) the α phase and (b) the β phase.

4. Experimental model validation

In order to estimate the accuracy of the developed surface generation model, three pockets, 20 μm in length and 5 μm in width, were machined by generating successive parallel grooves with the DNISP probe according to the set-up reported in table 4. The position of each pocket on the brass workpiece was such that they overlapped both the α and

β phases, as illustrated in figure 8. In addition, the cutting speed used was the same as that employed during the scratch tests and the applied force, F_n , was selected to ensure that cutting rather than ploughing took place along the length of the grooves.

Figure 9 compares the roughness profile predicted by the model when cutting through the α and β phases with a step-over value of 80 nm. From this figure, it can be

clearly seen that there is a difference between the predicted roughness profiles obtained when cutting the different phases. In particular, the maximum height achieved in the case of the α phase is lower than that obtained for the β phase under the same cutting conditions. This shows the significant effect of the material microstructure on the generated roughness during AFM probe-based mechanical machining of dual-phase materials.

The comparison between the predicted and experimentally measured data to assess the arithmetic surface roughness, R_a , for the three step-over values considered and for the different phases is illustrated in figure 10. However, it should be noted that, strictly speaking, the experimental R_a values measured should be referred to as P_a values since these are calculated from the primary profiles of the obtained AFM scans, where the long wave components have not been filtered out (Leach 2001). The reported experimental data represent the mean R_a values obtained from ten surface profile measurements for each phase and for each pocket. This figure shows that a relatively good agreement was achieved between the analytical and experimental results. Quantitatively, the average prediction error is 21%. This error was calculated as follows:

$$\text{error} = \frac{1}{n} \sum_{i=1}^n \left| \frac{R_{a\text{measured}} - R_{a\text{predicted}}}{R_{a\text{measured}}} \right|, \quad (3)$$

where n represents the total number of step-over conditions investigated. It can also be seen from this figure that the results given by the model generally tend to under-estimate the actual value of the arithmetic surface roughness. This is attributed to the fact that the developed model does not take into account the initial topography of the workpiece material and, thus, does not capture the profile waviness that can result from this original surface roughness. In particular, the model considers that the initial workpiece surface is perfectly flat, which is not a fully accurate assumption at nano-scale.

Finally, the average height between the bottom of a groove and its immediate neighbouring peak was calculated from ten measurements for each combination of step-over value and phase. The difference between the predicted results and the measured data were 23 and 28% for the α and β phase,

respectively. This discrepancy can be attributed to the fact that the model does not consider plastic side flow occurring at the side of the grooves.

5. Conclusions

The majority of existing research efforts that have focused on studying the topographical modification of a sample surface under the mechanical cutting action of an AFM probe have followed an experimental trial and error approach to achieve a particular process outcome. Thus, in comparison with the amount of experimental investigations, only a few studies have been directed at characterizing the process theoretically in order to improve its reliability and predictability. In this context, this paper reports on the development, implementation and testing of a new analytical model to predict the surface roughness generated when cutting pockets a few micrometres in width and a few tens of nanometres in depth with AFM probe-based machining. The distinguishing characteristic of the proposed model is that it takes into account the minimum chip thickness and elastic recovery associated with each phase present within the microstructure of a workpiece. The reported implementation consisted in determining the model material parameters and in validating its output when processing a dual phase brass alloy using an AFM nano-indentation probe. A relatively good agreement was achieved between the analytical and experimental results with an average prediction error of 21% when assessing the arithmetic average roughness, R_a . The predicted data generally under-estimated the experimental results and this is attributed to the fact that the model does not consider the initial surface roughness of the workpiece. In addition, future improvements of the model should also consider plastic flow at the side of the processed grooves. Thus, it is suggested that future work should focus on taking these factors into account in the model in order to improve its accuracy.

Acknowledgment

The reported research was funded by the Engineering and Physical Sciences Research Council (EPSRC) under the grants EP/I012133/1 and EP/F056745/1.

Appendix

Pseudo-code used to determine the coordinates of points along the roughness profile in the feed direction.

```

INITIALISE tip radius ( $r$ ), minimum chip thickness for each phase ( $\lambda_n$ ), elastic recovery value for each phase ( $k$ ), step-over ( $f$ )
and workpiece (microstructure map)

FOR EACH groove
  //Determine the coordinates of the tip centre  $O_i(X_{O_i}, Y_{O_i})$  based on  $r$  and  $f$ 
  CALCULATE  $X_{O_i}$  and  $Y_{O_i}$ 
  //Determine the coordinates ( $X_{P_i}, Y_{P_i}$ ) of each point  $P_{tc_i}$  along the tip profile
  CALCULATE  $X_{P_i}$ , and  $Y_{P_i}$ 
  DEFINE both intersection points with the preceding and follow-up profiles based on  $f$  and  $r$ 
  FOR ALL points ( $P_{tc_i}$ ) along the profile between the defined two intersection points
    DETERMINE the coordinates of the corresponding point ( $P_{tc_{i-1}}$ ) on the previous profile
    CALCULATE the distance between  $P_{tc_i}$  and  $P_{tc_{i-1}}$ 
    //Compare the results with the minimum chip thickness for the  $\alpha$  and the  $\beta$  phase
    IF distance  $> \lambda_n$  for the  $\alpha$  phase THEN
      //Cutting is the dominant mechanism
      KEEP the coordinates of  $P_{tc_i}$  to represent the resulting topography for the current
      groove
    ENDIF
    IF distance  $< \lambda_n$  for the  $\beta$  phase THEN
      //Ploughing is the prevailing mechanism and elastic recovery takes place
      Temporarily, REPLACE  $P_{tc_i}$  with  $P_{tc_{i-1}}$  to represent the resulting topography
      RETRIEVE the multiphase microstructure map to determine the phase type at the in-
      progress position
      IF phase =  $\beta$  THEN
        Final point on resulting topography =  $P_{tc_{i-1}} \times k$  for the  $\beta$  phase
      ENDIF
      IF phase =  $\alpha$  THEN
        Final point on resulting topography =  $P_{tc_{i-1}} \times k$  for the  $\alpha$  phase
      ENDIF
    ENDIF
    IF  $\lambda_n$  for the  $\beta$  phase  $<$  distance  $<$   $\lambda_n$  for the  $\alpha$  phase
    THEN
      //The dominant mechanism is dependent on the phase type
      RETRIEVE the multiphase microstructure map to determine the phase type at the in-
      progress position
      IF phase =  $\beta$  THEN
        //Cutting is the dominant mechanism
        KEEP the coordinates of  $P_{tc_i}$  to represent the resulting topography
      ENDIF
      IF phase =  $\alpha$  THEN
        //Ploughing is the prevailing mechanism and elastic recovery takes place
        Temporarily, REPLACE  $P_{tc_i}$  with  $P_{tc_{i-1}}$  to represent the resulting topography
        Final point on resulting topography =  $P_{tc_{i-1}} \times k$  for the  $\alpha$  phase
      ENDIF
    ENDIF
  ENDFOR
ENDFOR

CONSTRUCT the predicted surface profile based on the coordinates of the points stored

CALCULATE the surface roughness metric, Ra, based on the coordinates of all generated points

```

References

- Ahn B W and Lee S H 2009 Characterization and acoustic emission monitoring of AFM nanomachining *J. Micromech. Microeng.* **19** 045028
- Beegan D, Chowdhury S and Laugier M T 2007 Comparison between nanoindentation and scratch test hardness (scratch hardness) values of copper thin films on oxidised silicon substrates *Surf. Coat. Technol.* **201** 5804–8
- Binnig G, Quate C F and Gerber C 1986 Atomic force microscope *Phys. Rev. Lett.* **56** 930–4
- Blach J A, Watson G S, Brown C L, Pham D K, Wright J, Nicolau D V and Myhraa S 2004 A mechanistic approach to tip-induced nano-lithography of polymer surfaces *Thin Solid Films* **459** 95–9
- Bourne K, Kapoor S G and DeVor R E 2010 Study of a high performance AFM probe-based microscribing process *ASME Trans. J. Manuf. Sci. Eng.* **132** 030906
- Brammertz P H 1961 Ursachen fur formund massfehler an feinsbearbeiten werkstuechken *Dissertation T.H. Aachen*
- Brousseau E B, Krohs F, Caillaud E, Dimov S S, Gibaru O and Fatikow S 2010 Development of a novel process chain based on atomic force microscopy scratching for small and medium series production of polymer nano structured components *ASME Trans. J. Manuf. Sci. Eng.* **132** 030901
- Cheung C F and Lee W B 2000 Modelling and simulation of surface topography in ultra-precision diamond turning *Proc. Instn. Mech. Eng. B* **214** 463–80
- Cheung C F and Lee W B 2001 Characterisation of nanosurface generation in single-point diamond turning *Int. J. Mach. Tools Manuf.* **41** 851–75
- Chuzhoy L, DeVor R E and Kapoor S G 2003a Machining simulation of ductile iron and its constituents: part 2. Numerical simulation and experimental validation of machining *ASME Trans. J. Manuf. Sci. Eng.* **125** 192–201
- Chuzhoy L, DeVor R E, Kapoor S G, Beaudoin A J and Bammann D J 2003b Machining simulation of ductile iron and its constituents: part 1. Estimation of material model parameters and their validation *ASME Trans. J. Manuf. Sci. Eng.* **125** 181–91
- Donaldson R R and Patterson S R 1983 Design and construction of a large, vertical axis diamond turning machine *Proc. SPIE* **433** 62–7
- Dornfeld D, Min S and Yakeuchi Y 2006 Recent advances in mechanical micromachining *CIRP Ann.* **55** 745–68
- Elkaseer A M A, Dimov S S, Popov K B, Negm M and Minev R 2012 Modeling the material microstructure effects on the surface generation process in microendmilling of dual-phase materials *ASME Trans. J. Manuf. Sci. Eng.* **134** 044501
- Fang T H and Chang J 2003 Effects of AFM-based nanomachining process on aluminum surface *J. Phys. Chem. Solids* **64** 913–8
- Gozen B A and Ozdoganlar O B 2012 Design and evaluation of a mechanical nanomanufacturing system for nanomilling *Precis. Eng.* **36** 19–30
- Grzesik W 1996 A revised model for predicting surface roughness in turning *Wear* **194** 143–8
- Ikawa N, Shimada S and Tanaka H 1992 Minimum thickness of cut in micromachining *Nanotechnology* **3** 6–9
- Iwata F, Yamaguchi M and Sasaki A 2003 Nanometer-scale layer modification of polycarbonate surface by scratching with tip oscillation using an atomic force microscope *Wear* **254** 1050–5
- Komanduri R, Chandrasekaran N and Raff L M 2000 MD simulation of indentation and scratching of single crystal aluminium *Wear* **240** 113–43
- Leach R 2001 The measurement of surface texture using stylus instruments *National Physical Laboratory Good Practice Guide* vol 37 (Teddington, UK: National Physical Laboratory)
- Liu X, DeVor R E and Kapoor S G 2006 An analytical model for the prediction of minimum chip thickness in micromachining *ASME Trans. J. Manuf. Sci. Eng.* **128** 474–81
- Liu X, DeVor R E and Kapoor S G 2007 Model-based analysis of the surface generation in microendmilling—part I. Model development *ASME Trans. J. Manuf. Sci. Eng.* **129** 453–60
- Liu X, DeVor R E, Kapoor S G and Ehmann K F 2004 The mechanics of machining at the micro-scale: assessment of the current state of the science *ASME Trans. J. Manuf. Sci. Eng.* **126** 666–78
- Liu K and Melkote S N 2006 Effect of plastic side flow on surface roughness in micro-turning process *Int. J. Mach. Tools Manuf.* **46** 1778–85
- Luo X, Cheng K, Guo X and Holt R 2003 An investigation on the mechanics of nanometric cutting and the development of its test-bed *Int. J. Prod. Res.* **41** 1449–65
- Luo X, Cheng K and Ward R 2005 The effects of machining process variables and tooling characterisation on the surface generation *Int. J. Adv. Manuf. Technol.* **25** 1089–97
- Mian A, Driver N and Mativenga P T 2010 A comparative study of material phase effects on micro-machinability of multiphase materials *Int. J. Adv. Manuf. Technol.* **50** 163–74
- Simoneau A, Ng E and Elbestawi M A 2006 The effect of microstructure on chip formation and surface defects in microscale, mesoscale, and macroscale cutting of steel *CIRP Ann.* **55** 97–102
- Son S M, Lim H S and Ahn J H 2005 Effects of friction coefficient on the minimum cutting thickness in micro cutting *Int. J. Mach. Tools Manuf.* **45** 529–35
- Sundararajana S and Bhushan B 2001 Development of a continuous microscratch technique in an atomic force microscope and its application to study scratch resistance of ultrathin hard amorphous carbon coatings *J. Mater. Res.* **16** 437–45
- Tseng A A, Kuo C-F J, Jou S, Nishimura S and Shirakashi J-I 2011 Scratch direction and threshold force in nanoscale scratching using atomic force microscopes *Appl. Surf. Sci.* **257** 9243–50
- Vogler M P, DeVor R E and Kapoor S G 2003 Microstructure-level force prediction model for micro-milling of multi-phase materials *ASME J. Manuf. Sci. Eng.* **125** 202–9
- Vogler M P, DeVor R E and Kapoor S G 2004 On the modeling and analysis of machining performance in micro-endmilling: part 1. Surface generation *ASME Trans. J. Manuf. Sci. Eng.* **126** 685–94
- Wang J, Gong Y, Abba G, Chen K, Shi J and Cai G 2008 Surface generation analysis in micro end milling considering the influences of grain *Microsyst. Technol.* **14** 937–42
- Weule H, Huntrup V and Tritschle H 2001 Micro-cutting of steel to meet new requirements in miniaturisation *CIRP Ann.* **50** 61–4
- Wills-Moren W J, Modjarrad H, Read R F and McKeown P A 1982 Some aspects of the design and development of a large high precision CNC diamond turning machine *CIRP Ann.* **31** 409–14
- Yan Y D, Sun T, Liang Y C and Dong S 2009 Effects of scratching directions on AFM-based abrasive abrasion process *Tribol. Int.* **42** 66–70
- Ye Y Y, Biswas R, Morris J R, Bastawros A and Chandra A 2003 Molecular dynamics simulation of nanoscale machining of copper *Nanotechnology* **14** 390–6
- Zhang L and Tanaka H 1997 Towards a deeper understanding of wear and friction on the atomic scale—a molecular dynamics analysis *Wear* **211** 44–53
- Zhou L and Cheng K 2009 Dynamic cutting process modelling and its impact on the generation of surface topography and texture in nano/micro cutting *Proc. Inst. Mech. Eng. B* **223** 247–66